GROUND-BASED NETWORK VERIFICATION OF GOMOS OZONE PROFILE DATA v 7.0cd (BASELINE 2008) VERSUS v 6.0cf

Vandenbussche S., C. De Clercq, J. Granville, J.-C. Lambert,
and the Multi-TASTE Ozone Profile Team

Belgian Institute for Space Aeronomy, Brussels, Belgium

Scope of this document

This document reports on the verification of GOMOS ozone processor upgrade from version 6.0cf to version 7.0cd (also referred to as baseline algorithm 2008) based on comparisons with ground-based network data. GOMOS ozone profile data subsets selected for this verification exercise and processed at ACRI have been compared to correlative observations collected from ground-based networks of ozonesonde and lidar stations affiliated with WMO's Global Atmosphere Watch and contributing networks, i.e. the Network for the Detection of Atmospheric Composition Change (NDACC) and Southern Hemisphere ADditional OZonesondes (SHADOZ). GOMOS data retrieved with the reference version of the processor (6.0cf) had already been shown to agree quite well, in the stratosphere, with correlative measurements (within a few percents). However, at high North latitudes, a negative bias of about 10 % was present in GOMOS 6.0cf data. In the lower stratosphere (near the tropopause), the relative difference between GOMOS 6.0cf data and correlative measurements increases rapidly with decreasing altitude, to reach more than 50 % in the troposphere.

Verification method

GOMOS and correlative observations have been selected using basic space and time co-location criteria: the maximum distance allowed between the GOMOS tangent point and the station is 500 km, and the maximum time distance allowed between GOMOS and correlative data is 6 h (for comparisons with night-time lidar data) or 12 h (for comparisons with daytime ozonesonde data). More accurate selection methods exist, however, given the amount of GOMOS profiles available for this verification and given the horizontal resolutions of the satellite and ground-based measurements, a maximum distance of 500 km was found as the best compromise between a sufficient coincidence of the air masses to be compared and a sufficient amount of collocated pairs of profiles.

Star occultations measured by GOMOS under full dark conditions ("PCD_ILLUM" = 0, referred to as "dark data" in this document) and under straylight conditions ("PCD_ILLUM" = 3, referred to as "straylight data" in this document) were both used in this verification. Indeed, at Northern high latitudes stations (beyond 50°), GOMOS data recorded under straylight conditions only are available. At Northern middle latitude stations, the dark data set is quite small with respect

to the straylight data set. At South latitudes, nearly only dark GOMOS profiles are available in the data set.

In our study, when both dark and straylight GOMOS data are available at one station (typically at middle latitudes), the separate study of both data sets shows that they lead to qualitatively equivalent results for a coincident time period. Furthermore, data recorded under straylight conditions is reported in the Product Handbook (ESA GOMOS Product Handbook version 3, 31 May 2007, available online: http://envisat.esa.int/handbooks/gomos/toc.htm) to be of "good quality". Therefore, to increase the amount of comparisons with ground-based measurements, dark and straylight data comparisons have been merged for our study, when this merging increased significantly the number of comparisons (typically at middle latitudes). The selected illumination condition(s) is mentioned in the title of each figure. Twilight data ("PCD_ILLUM" = 2 or 4) were found to be of lower quality (as reported in the Product Handbook) and is not used in this verification. Bright limb conditions data ("PCD_ILLUM" = 1) is also not used in this study, as they are reported to be of "quite bad quality" in the Product Handbook.

Each ground-based profile collocated with a GOMOS profile was integrated into partial columns around the altitudes of the corresponding GOMOS profile. Then each partial column was divided by its height to obtain ozone number densities. After that, in order to keep the same altitude grid for all data, all ground-based and GOMOS profiles were linearly interpolated to the altitude grid of 0 to 60 km (1 km step).

The error bars reported in the GOMOS files were used to remove data having a very high uncertainty. No additional filtering based e.g. on quality flags was applied. The two versions of the GOMOS processor (GOPR) report different error bars: the reference version v6.0cf generates relative error values, while the new prototype v7.0cd generates absolute error values in an internal unit. These absolute error values were converted in ozone number density units using the following formula (following an E-mail from Gilbert Barrot (ACRI) to the GOMOS QWG mailing list in November 2008): ABS_ERR = 10 exp(0.05*err_in_file). To enable comparative studies, we converted these absolute errors into relative errors by dividing them by the corresponding ozone profile number density values. These relative error values were treated as the ozone profile data (i.e. integrated in partial columns, divided by the height and interpolated to the same altitude grid). For both versions of the processor, data for which the reported relative error exceeded 500 % were removed. If less than five data points on the interpolated altitude grid were concerned, only the concerned data points were removed from the analysis. Otherwise, the complete profile was removed from the analysis.

General analysis of time series

The first part of this study consists of the visual inspection and statistical studies of GOMOS ozone profile time-series, of collocated ground-based measurements, and of their relative difference. The objective is to identify possible global features, cyclic errors, and long-term drifts.

Figures 1 to 8 show time series at different ozonesonde and lidar stations. The figures on the left (the "*a"* serie) are for the new prototype v7.0cd of the processor, and the figures on the right (the "*b*" serie) are for the reference version v6.0cf of the processor. In each figure, the first subplot shows the time series of the ozone number density profile measured by GOMOS within 500 km around the ground-based station. The second subplot shows the same time series as sounded at the station by ozonesonde or by lidar. The third subplot shows the relative difference between GOMOS and ground-based time series for collocated

measurement events. For a better visibility, a one-month running mean[1] has been applied to the three time series.

Unless stated otherwise, the behaviour illustrated in these figures is typical of that observed at other stations in the same latitude zones.

The qualitative comparison of GOMOS ozone profile time series shows that GOMOS profiles have a correct vertical shape and that they capture well the annual variation of stratospheric ozone down to about 18 km. The relative differences between GOMOS and correlative measurements obtained with the new GOPR prototype are very similar to the ones obtained with the previous processor version 6.0cf.

At middle latitudes, the mean difference between GOMOS and collocated ground-based measurements in the stratosphere reaches only a few percent in both dark and straylight GOMOS data (see for example Figure 4 at Payerne in the Swiss Alps, and Figure 7 in Haute Provence in Southern France). Below the tropopause, mean relative differences are large and exceed 50 %.

A negative bias of about 5 to 10 %, already pointed out in version 6.0cf, persists at high North latitudes in the straylight GOMOS data (no dark data available), as illustrated in Figures 1 and 2. The value of this bias diminishes with decreasing latitudes, to reach 0 at about 50°N. This bias stays of the same order of magnitude as in the previous version of the processor (6.0cf).

At Hohenpeißenberg in Germany, the comparison between GOMOS dark and straylight data and correlative lidar or ozonesonde data (Figure 3) reveals a negative bias in the stratosphere that seems to arise with time, for both versions of the processor. This trend is not observed in time series of comparisons at other mid-latitude stations.

At the equatorial station of Paramaribo (Figure 5), a negative bias seems to be present in GOMOS data from about 25 to 35 km. However, this cannot be confirmed because no collocated data is available at other equatorial stations.

At Marambio in Antarctica (Figure 6), GOMOS data seems to capture the low ozone concentration during the ozone hole (dark data, no straylight data available), but there are too few collocated data at this station during ozone hole events to conclude quantitatively.

[1] For each day, an “average” measurement is calculated using a Gaussian-weighted window centered on this day, calibrated so that 3σ correspond to 15 days (i.e. 99.75 % of the Gaussian integral lies in a 30 days interval)

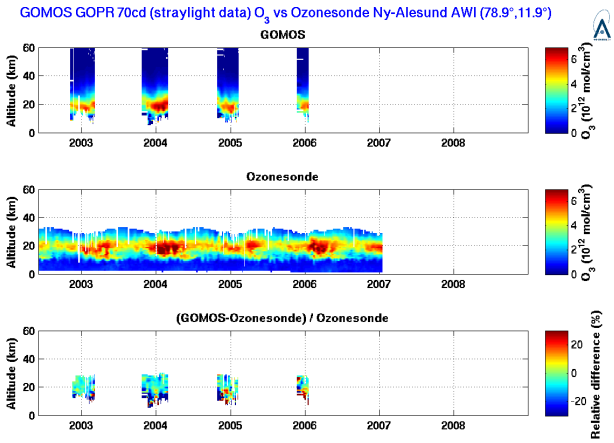

***Figure 1a**: Time series of GOMOS **(GOPR 7.0cd)** ozone profile concentration around Ny-Ålesund, Spitsbergen (top). Corresponding time series of the ozone profile probed by AWI ozonesondes lauched from Ny-Ålesund (centre). Time series of the relative difference between GOMOS and ozonesonde ozone profile data (bottom).*

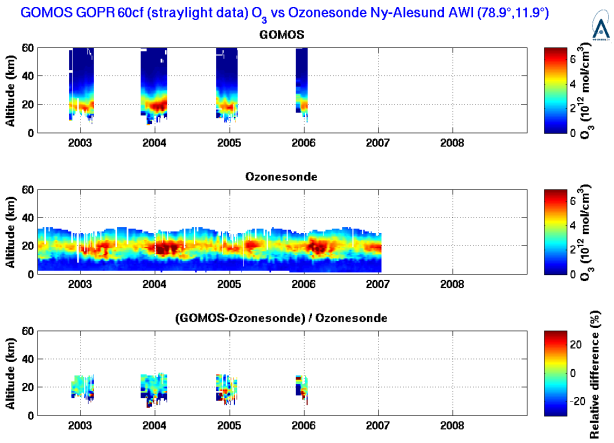

Figure 1b**: Same as Figure 1a but for the reference GOMOS processor **(GOPR 6.0cf)

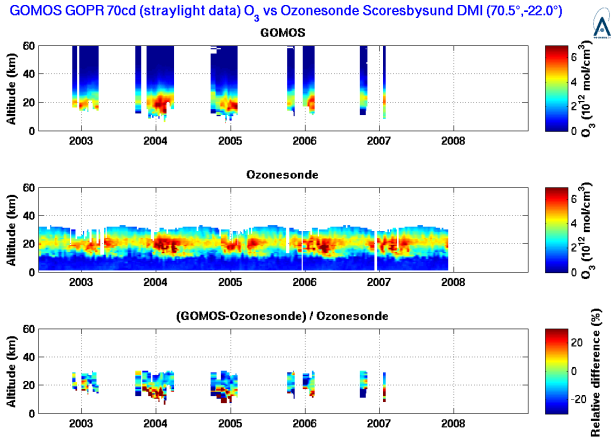

***Figure 2a**: Same as Figure 1a, but at the DMI ozonesonde station of Scoresbysund in Eastern Greenland.*

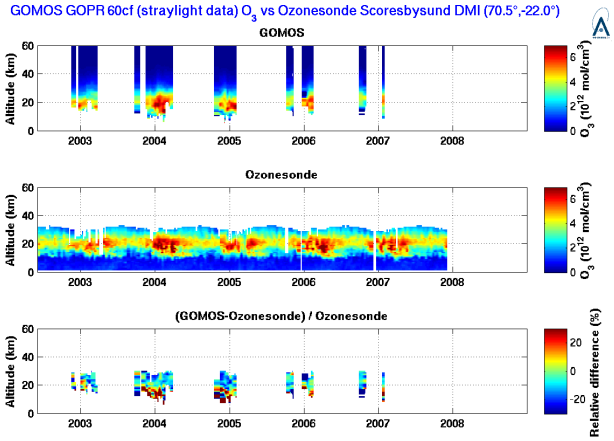

Figure 2b**: Same as Figure 2a but for the reference GOMOS processor **(GOPR 6.0cf)

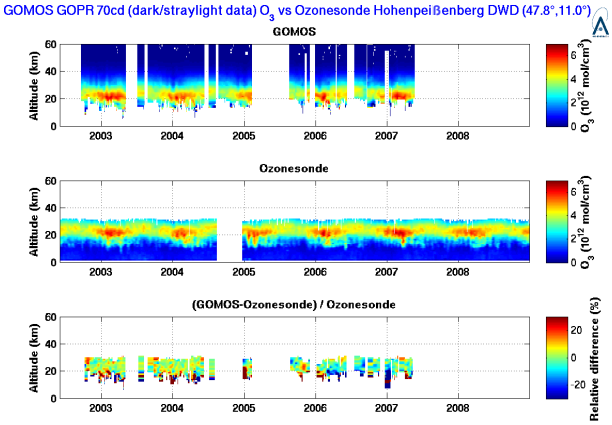

***Figure 3a**: Same as Figure 1a, but at the DWD ozonesonde station of Hohenpeißenberg in Germany.*

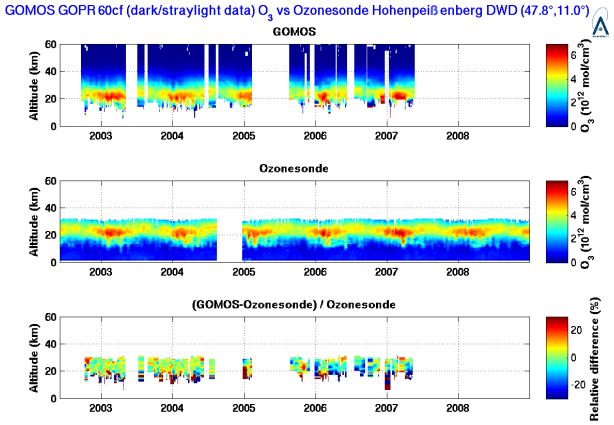

Figure 3b**: Same as Figure 3a but for the reference GOMOS processor **(GOPR 6.0cf)

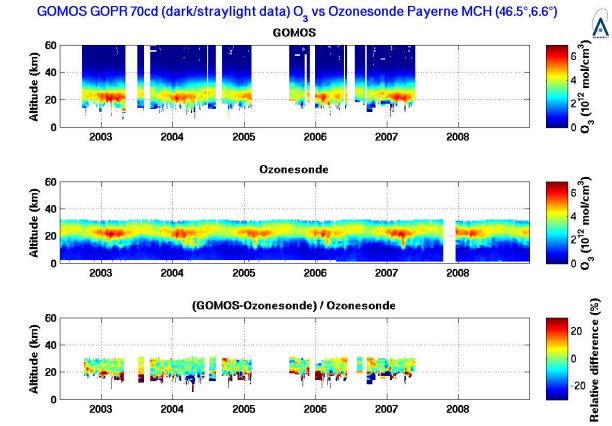

***Figure 4a**: Same as Figure 1a, but at the MCH ozonesonde station of Payerne in the Swiss Alps.*

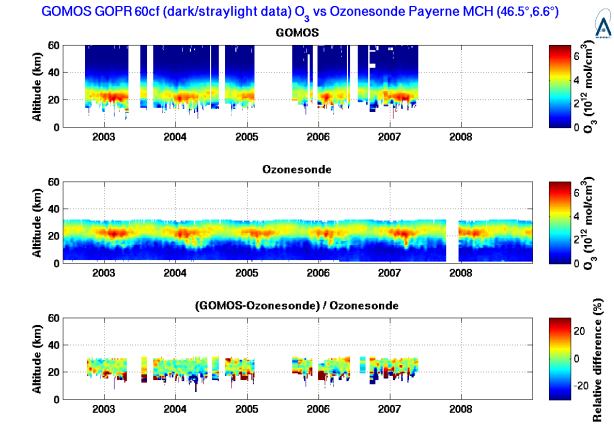

Figure 4b**: Same as Figure 4a but for the reference GOMOS processor **(GOPR 6.0cf)

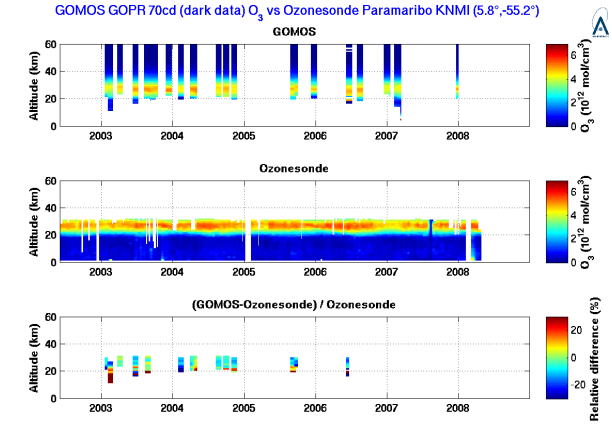

***Figure 5a**: Same as Figure 1a, but at the KNMI ozonesonde station of Paramaribo in Surinam.*

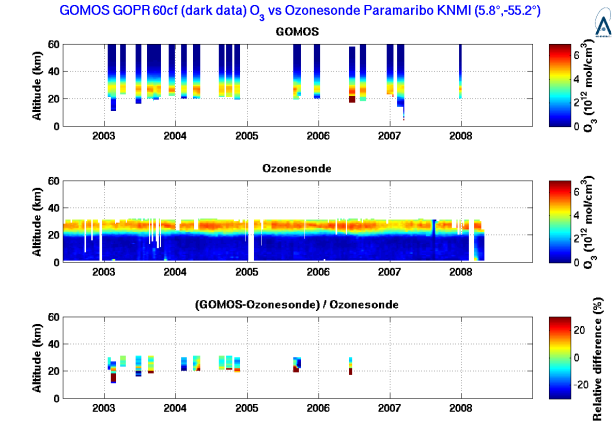

Figure 5b**: Same as Figure 5a but for the reference GOMOS processor **(GOPR 6.0cf)

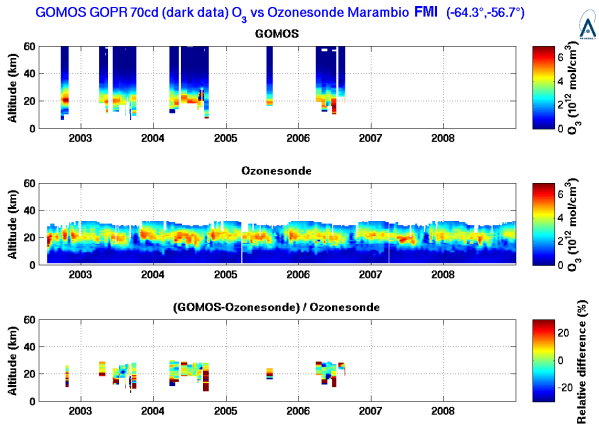

Figure 6a: *Same as Figure 1a, but at the INTA ozonesonde station of Marambio in the Antarctic peninsula.*

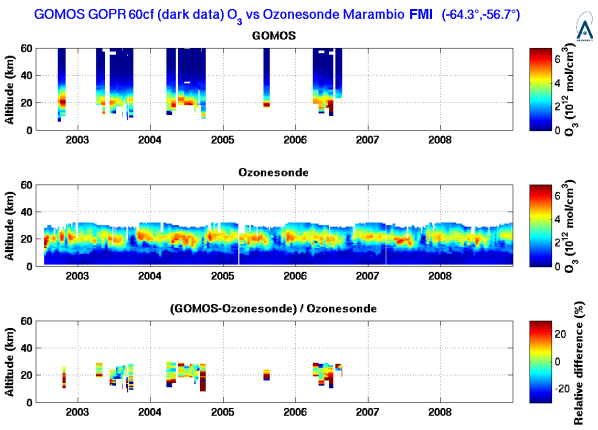

Figure 6b*: Same as Figure 6a but for the reference GOMOS processor* ***(GOPR 6.0cf)***

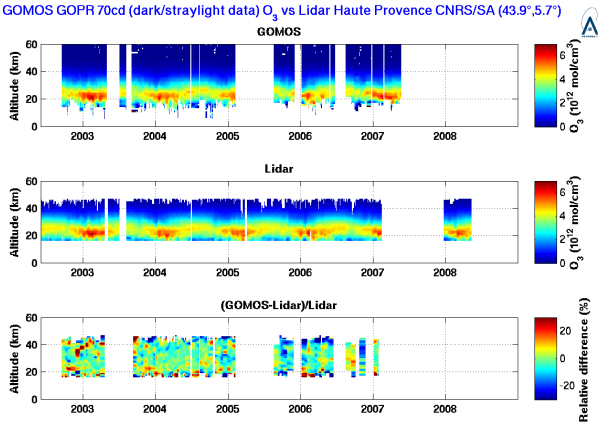

Figure 7a*: Same as Figure 1a, but at the CNRS lidar station of Observatoire de Haute Provence in Southern France.*

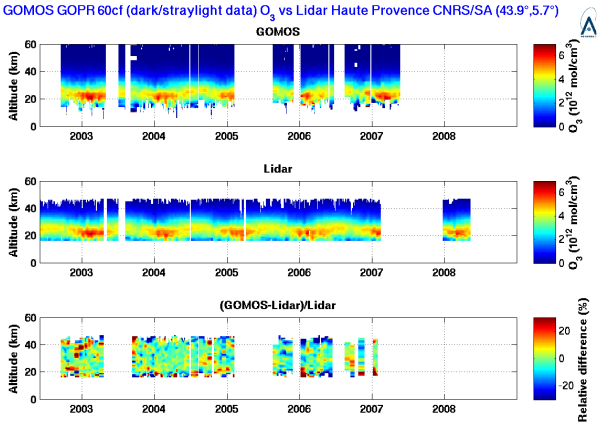

Figure 7b*: Same as Figure 7a but for the reference GOMOS processor* ***(GOPR 6.0cf)***

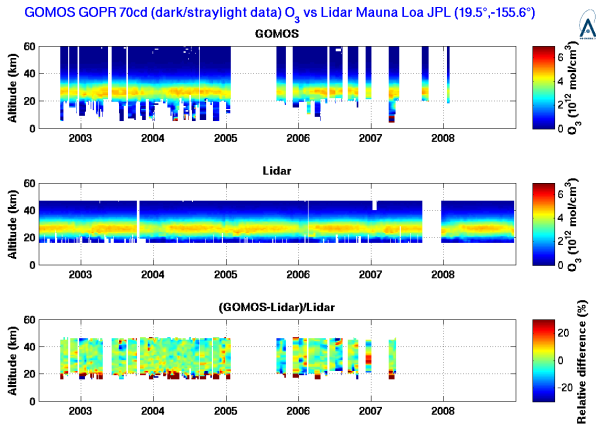

Figure 8a: *Same as Figure 1a but at the JPL lidar station of Mauna Loa on Big Island, Hawaii.*

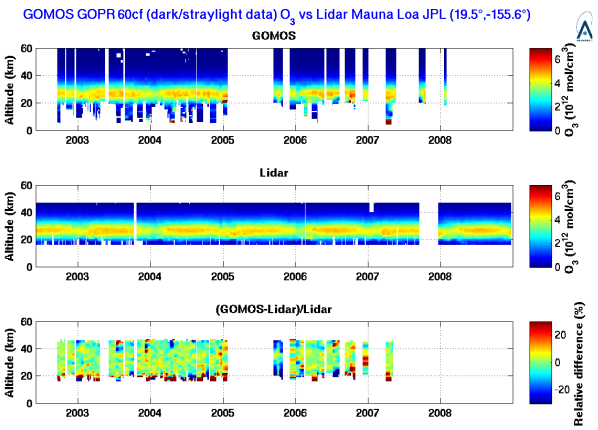

Figure 8b: *Same as Figure 6a but for the reference GOMOS processor* ***(GOPR 6.0cf)***

Analysis of long term drifts

In order to detect and quantify long-term drifts of GOMOS data with respect to long-term quality controlled ground-based networks, the relative difference between GOMOS and ground-based measurements has been plotted as a function of the time, at different altitudes. The mean and standard deviation of these relative differences are displayed on each plot (μ and σ respectively). Bias of more than 1 % ($\mu > 1$ %) are shown in red. Except when the standard deviation on the data was higher than 30 %, a linear regression was applied, using a modified least squares method which allocates a smaller weight to the outsiders. The slope of the regression is displayed on each plot (α) together with its 95 % confidence interval. Significant trends (zero is not inside the 95% confidence interval of the slope) are highlighted in red.

At most stations and in particular for the dark conditions, the data set does not cover a long time period with sufficient sampling for analysing long-term trends, and the conclusions drawn here should not be considered general. Below 20 km, the standard deviation of the agreement between GOMOS and ground-based measurements is very large, and no regression was performed.

Our analysis confirms that, for both versions of the processor, a negative bias of about 5 to 10 % exists at Northern high latitudes, and diminishes with decreasing latitude to reach 0 at about 50°N. At some stations, the bias seems to be reduced (by about 1 to 2 %, depending on the location) with the new version of the processor with respect to the old version. However, at other stations this bias is increased by the same amount in the new prototype of the processor. We should therefore not consider this as significant. In the intertropical region and to 45°S, a positive bias of about 5 % at 20 km seems to be present, for both versions of the GOMOS processor. However, this must be considered with precaution because a sufficient time series of collocations exists for only 3 stations in this geographical area (Table Mountain, 34.2°N; Mauna Loa, 19.5°N; Lauder, 45°S).

Long-term drifts have been detected at some stations. However, the drift estimates do not match for different stations in the same latitude zone. For example, a negative trend is detected in this analysis at the German station of Hohenpeißenberg (about -3 % / year at 20 km) and at the French lidar station of Haute Provence (about -2 % per year at 20 km), but no significant trend is observed in Uccle in Belgium and Payerne in Switzerland.

At the stations where long-term drifts have been detected, the difference in the trend for data obtained by the two GOMOS processors compared in this study is not significant: this difference is usually less than the standard deviation on the trend.

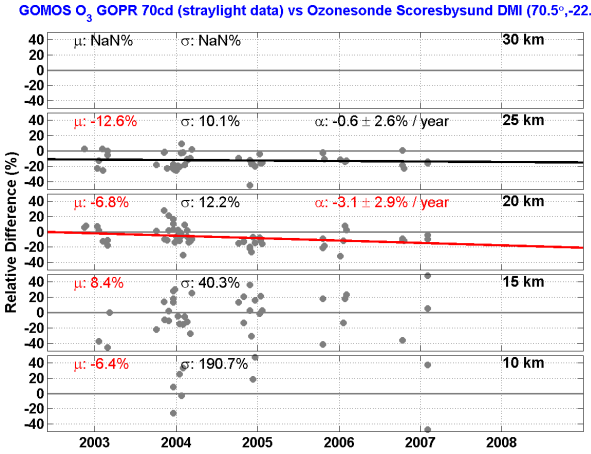

***Figure 9a**: Time series of the difference between GOMOS **(GOPR 7.0cd)** and ground-based ozone number density measured around the DMI ozonesonde station of Scoresbysund in Eastern Greenland, at different altitudes.*

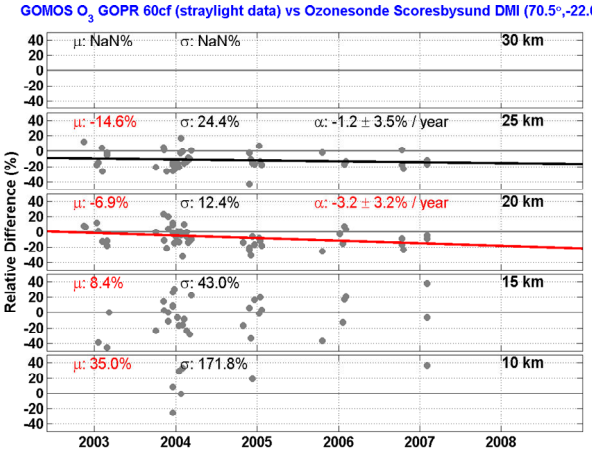

Figure 9b**: Same as Figure 9a, but for the reference GOMOS processor **(GOPR 6.0cf).

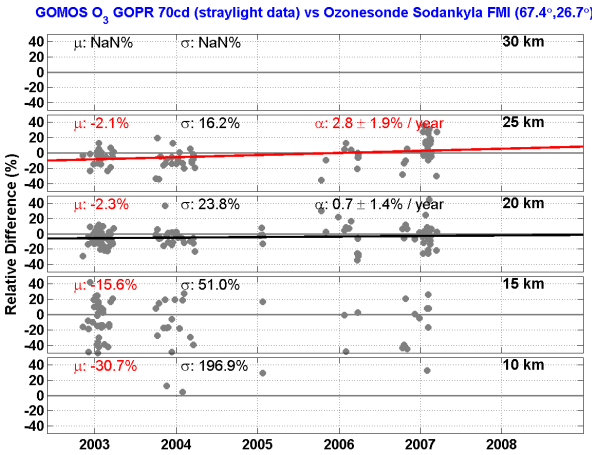

***Figure 10a**: Same as Figure 9a, but at the FMI ozonesonde station of Sodankylä (Finland).*

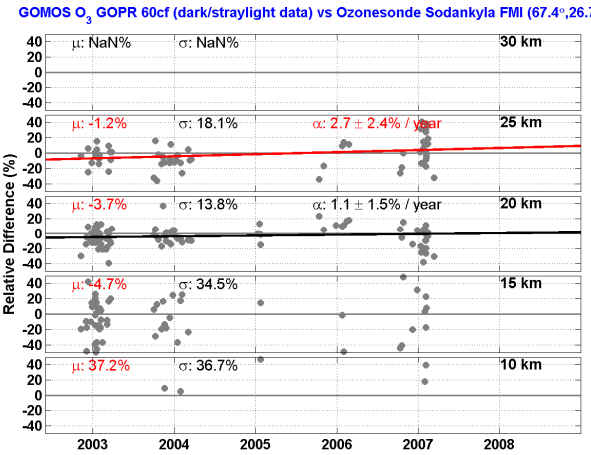

Figure 10b**: Same as Figure 10a, but for the reference GOMOS processor **(GOPR 6.0cf).

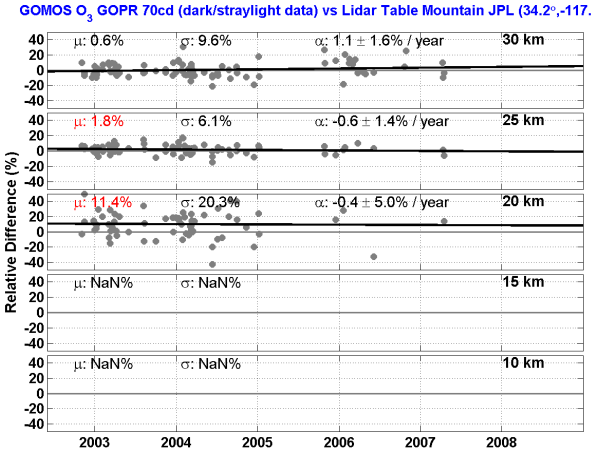

***Figure 11a**: Same as Figure 9a, but at the JPL lidar station of Table Mountain (California, USA).*

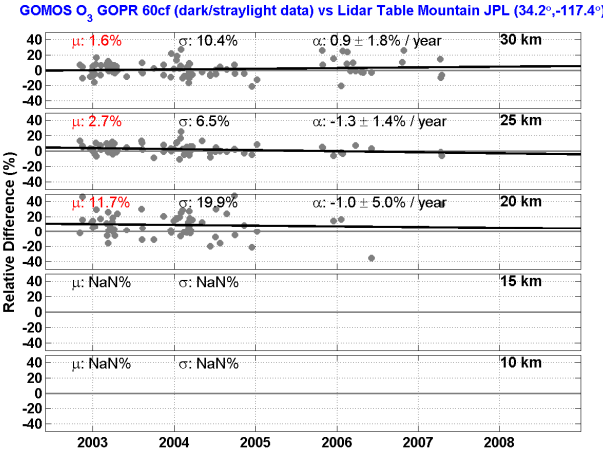

Figure 11b**: Same as Figure 11a, but for the reference GOMOS processor **(GOPR 6.0cf).

Statistical analysis of vertical structures

The global stability of the mean GOMOS/ground agreement along the 2002-2008 time period allows us to carry out the second part of our study: the tentative statistical analysis of the agreement between GOMOS and correlative ozone profile measurements over the entire timeframe.

To determine the best statistical estimates, the statistical distribution of the relative difference between GOMOS and ground-based measurements was studied, for both data processors. Figures 12 to 15 show, at different altitudes, this statistical distribution for the new prototype of the processor (in red) and for the reference version (in blue). The first and last bars of each histogram contain all the data for which a relative difference of more than 30 % is present (negative or positive for the first and last bar respectively). The mean (μ) and standard deviation (σ) are displayed on the figures at each altitude. The figures also display the median (m) and the inter-percentile (IP) interval corresponding to 68% of the results (ie: difference between percentile 84 and percentile 16), to be comparable with the standard deviation. At each altitude, the Gaussian curve corresponding to the mean and standard deviation of the data set is represented on the figure. On each figure, the number of collocated profiles is indicated. At altitudes where less than five collocated measurements are available, the corresponding histogram(s) is/are not displayed.

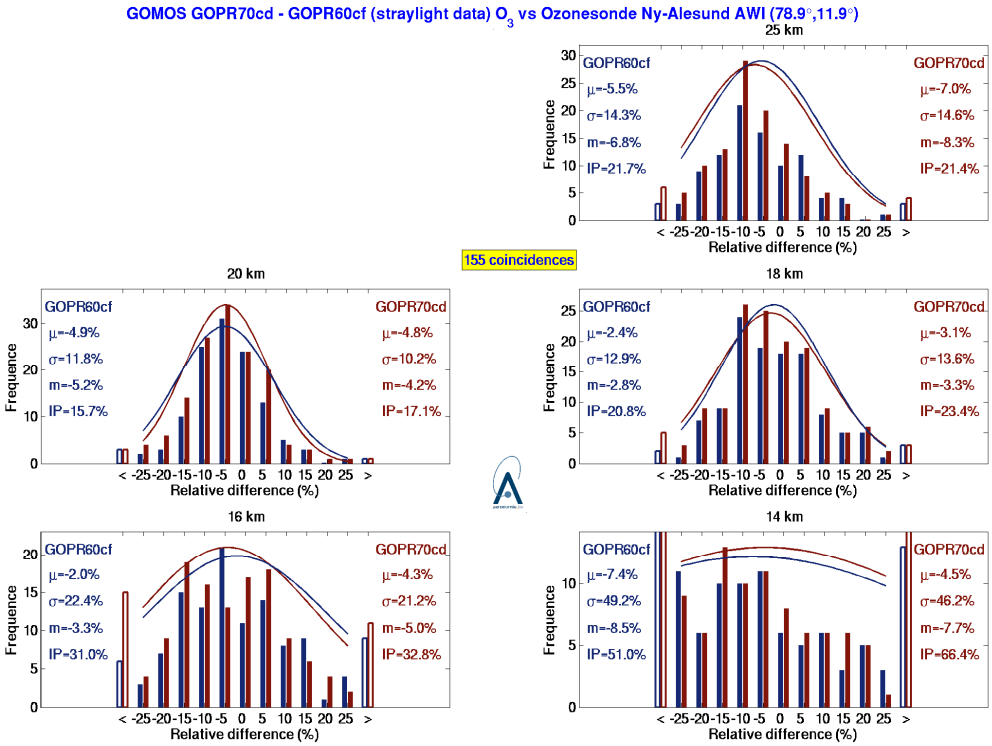

***Figure 12**: Statistical distribution of the relative difference between GOMOS and ground-base ozone number density measured, at different altitudes, at the AWI ozonesonde station of Ny-Ålesund in Norway. GOMOS v6.0cf in blue and v7.0cd in red.*

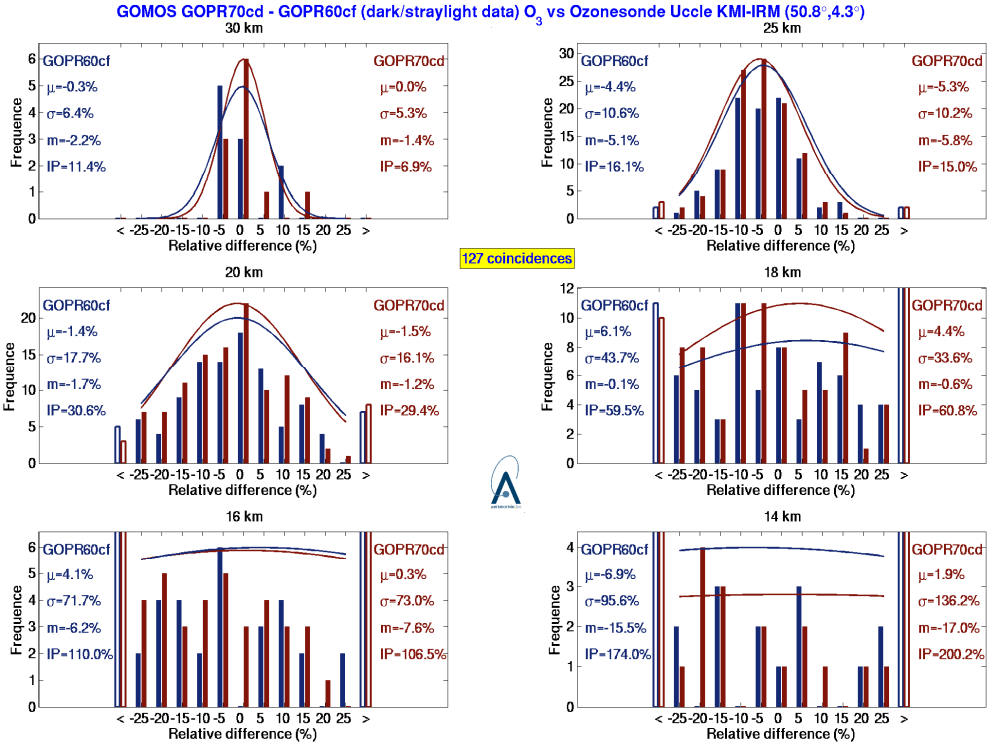

***Figure 13**: Same as Figure 12, but at the RMI ozonesonde station of Uccle in Belgium.*

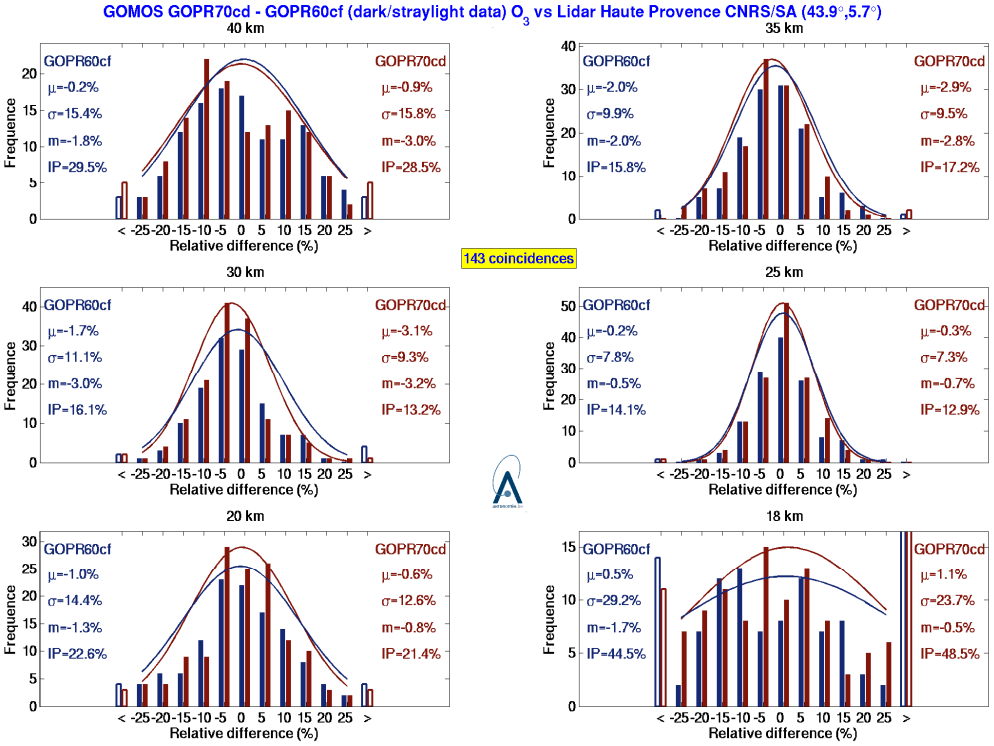

***Figure 14**: Same as Figure 12, but at the CNRS lidar station of Haute Provence in southern France.*

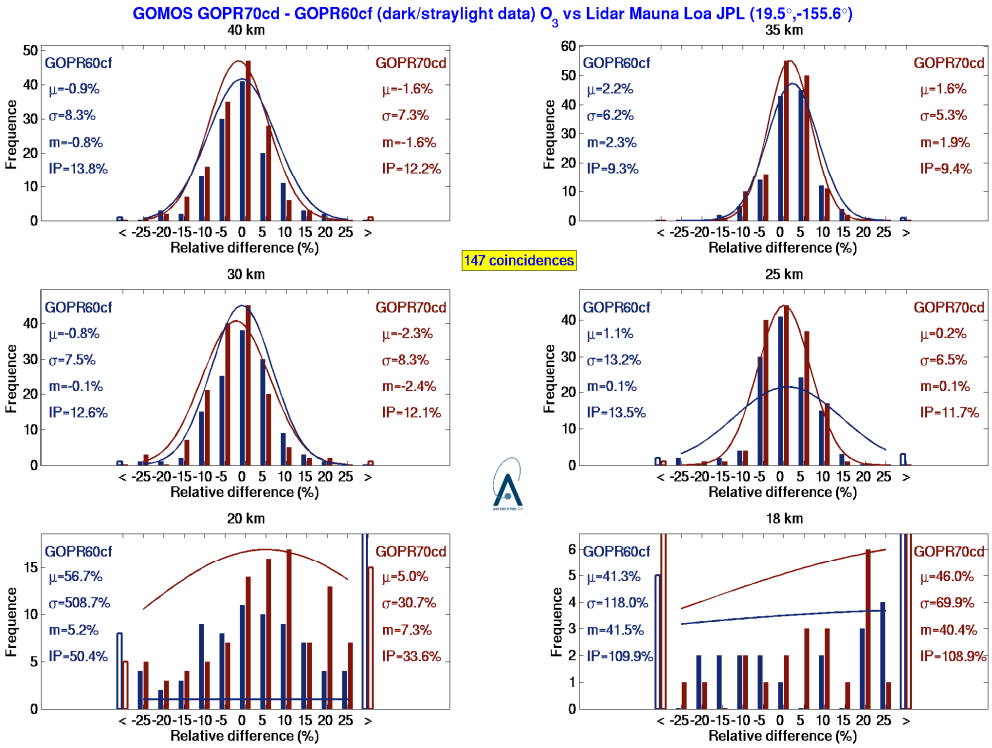

***Figure 15**: Same as Figure 12, but at the JPL lidar station of Mauna Loa in Hawaii.*

In general, from altitudes of 35 km down to a few kilometres above the tropopause, the statistical dispersion of the relative differences is close to a Gaussian curve, provided that a sufficient amount of collocations exists (at least 40). Below those altitudes, the distribution of the relative differences shows a large proportion of data for which this difference is more than +/- 30 %. The study of the mean of all relative differences (between GOMOS and collocated ground-based profiles) at a station is only relevant in the altitude levels where the statistical distribution of the differences approaches a Gaussian curve. The number of stations where more than 40 time collocations with GOMOS dark or straylight measurements exist in the data set is quite limited.

In order to detect an improvement of the vertical profile data obtained with the new version of the GOMOS processor 7.0cd with respect to the reference version 6.0cf, we plotted the mean and standard deviation of the relative differences between GOMOS and ground-based collocated measurements as a function of the altitude. The data for both versions of the data processor are displayed on the same graphics: the new version 7.0cd in red, and the old version 6.0cf in blue. On the second panel of each graph, the mean and standard deviation (added to the mean) of the relative error bars on the original GOMOS data are shown. Errors attributed to ground-based measurements are also displayed in black on these graphics. For ozone sondes, no error bars are currently available, and the error has been assumed to be of 7.5 +/- 4 % (Smit et al., JGR 112, D19306, 2007). Figures 16 to 19 show these graphs for the stations at which the statistical distribution of the relative differences have been shown in Figures 12 to 15. Figures 20 to 23 display the same plots, for stations with less coincident data but where a higher difference is observed between the two GOMOS processors.

Our analysis confirms again the high North latitudes bias of about 10 %, for both versions of the processor. In the stratosphere, the 1σ standard deviation of the differences is of the order

of 10 to 20 %. Mean differences increase rapidly from the UTLS to lower altitudes, with a standard deviation of more than 50 %.

At most stations, the agreement between GOMOS (GOPR 7.0cd) and ground-based measurements is slightly better (maximum a few percent, not uniform) in the lower stratosphere (from 15-20 km to about 25 km) than with the previous processor version 6.0cf. At lower altitudes, the relative difference between GOMOS and ground-based data is still large and, as shown before, the distribution of this difference data is far from a Gaussian curve, mean and standard deviation are not meaningful parameters of the distribution.

At most stations, a negative shift (usually 1 %, up to 3% in some cases) is observed from 25 - 30 km to higher altitudes, between ozone number densities retrieved with the new version of the processor and the reference version. This shift yields better comparison results at some stations, but also worse comparison results at other stations. This also varies with the altitude.

At the FMI ozonesonde station of Sodankylä in Finland, the data from the new prototype of the processor seems to differ more from the ground-based data than the data from the old version of the processor, from about 10 to about 18 km altitude. However, such a behaviour was only noticed at this station.

The reported error bars on the data (converted in relative values for the new prototype of the processor) are largely lower with the new version of the processor, from about 25 to 45 km altitude. However, this does not seem to reflect on the comparison statistics. In most cases, these error bars are also slightly better at lower altitudes with the new prototype of the processor.

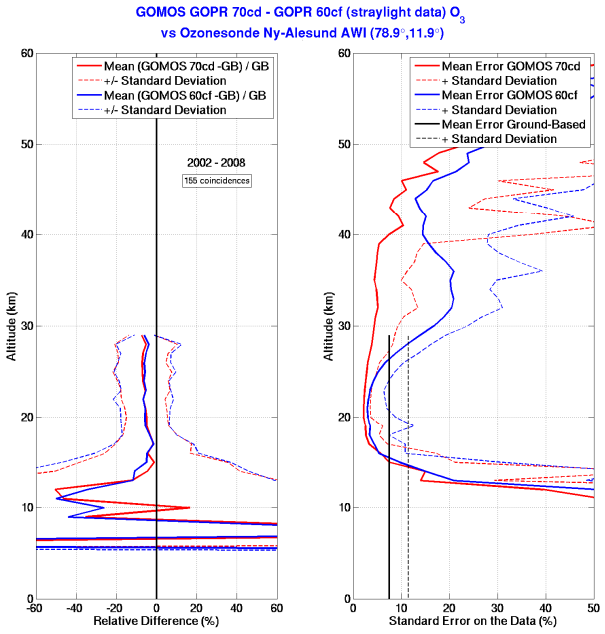

***Figure 16**: First panel: relative difference between GOMOS (GOPR 7.0cd in red, GOPR 6.0cf in blue) and ground-based ozone profiles at the AWI ozonesonde station of Ny-Ålesund, as a function of altitude. Second panel: mean of the relative errors for GOMOS and ground-based measurements used in the comparisons. Details can be found in the text.*

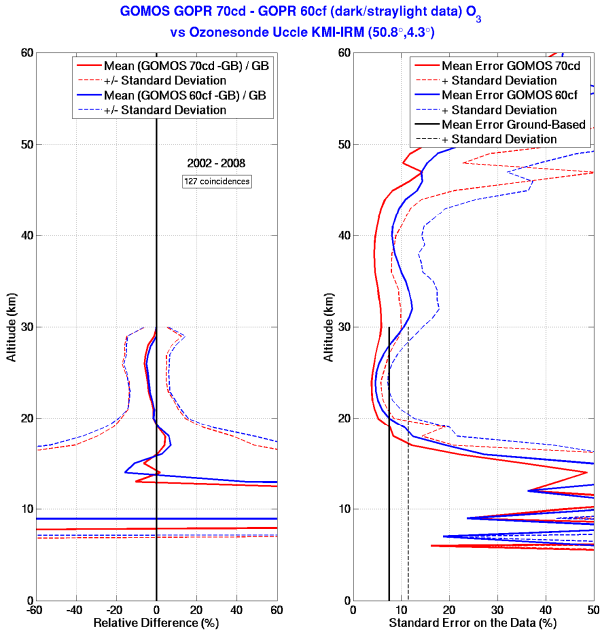

***Figure 17**: Same as Figure 16, but at the RMI ozonesonde station of Uccle in Belgium.*

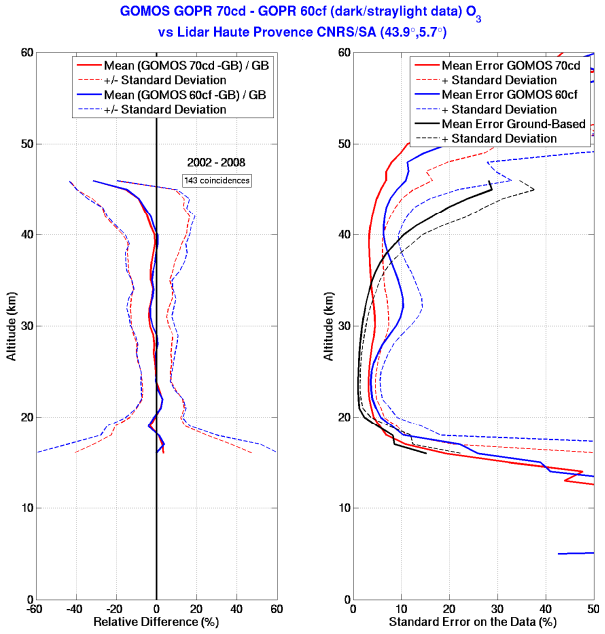

***Figure 18**: Same as Figure 16, but at the CNRS lidar station in Haute Provence, southern France.*

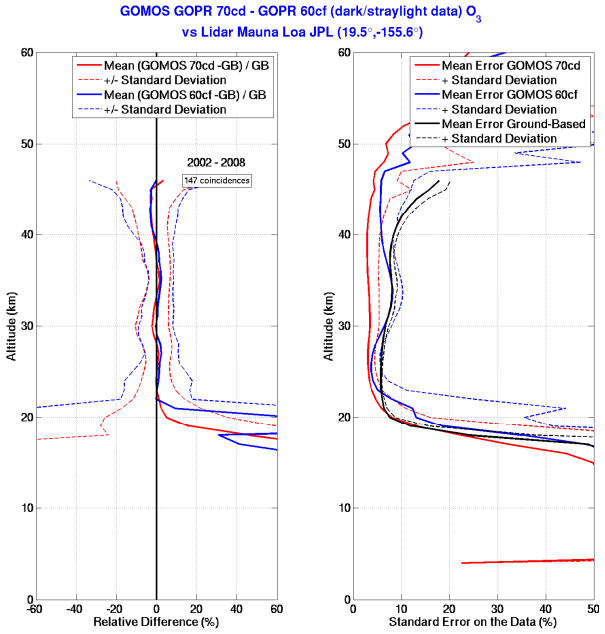

***Figure 19**: Same as Figure 16, but at the JPL lidar station of Mauna Loa, Hawaai.*

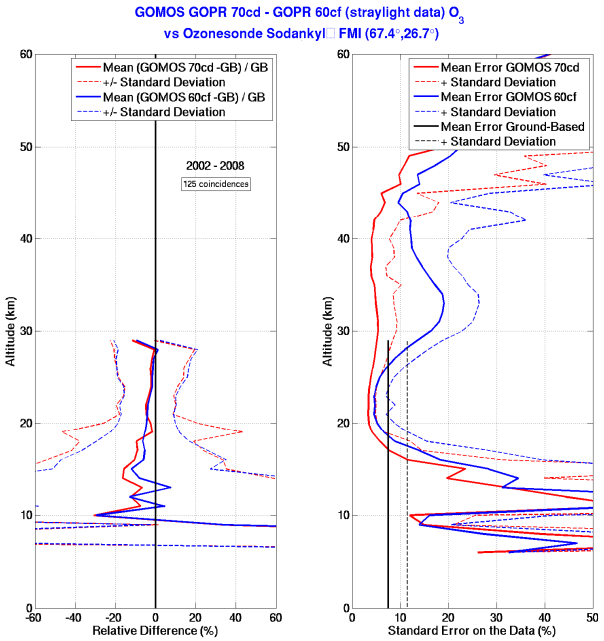

***Figure 20**: Same as Figure 16, but at the FMI ozonesonde station in Sodankyla, Finland.*

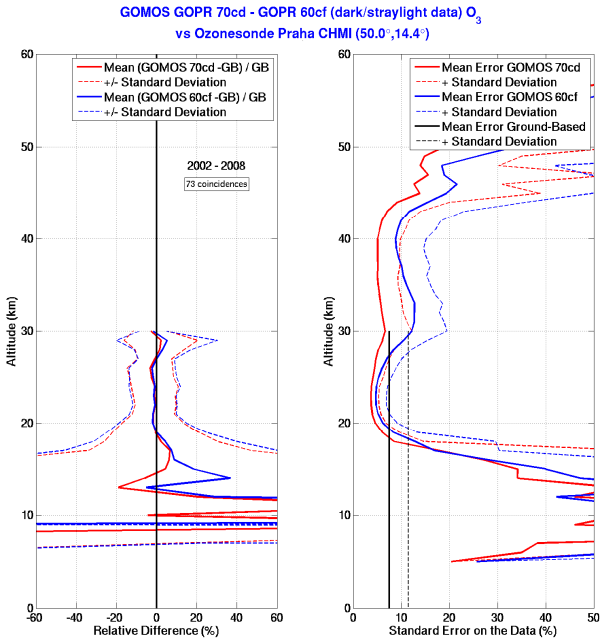

***Figure 21**: Same as Figure 16, but at the CHMI ozonesonde station in Praha, Czech Republic.*

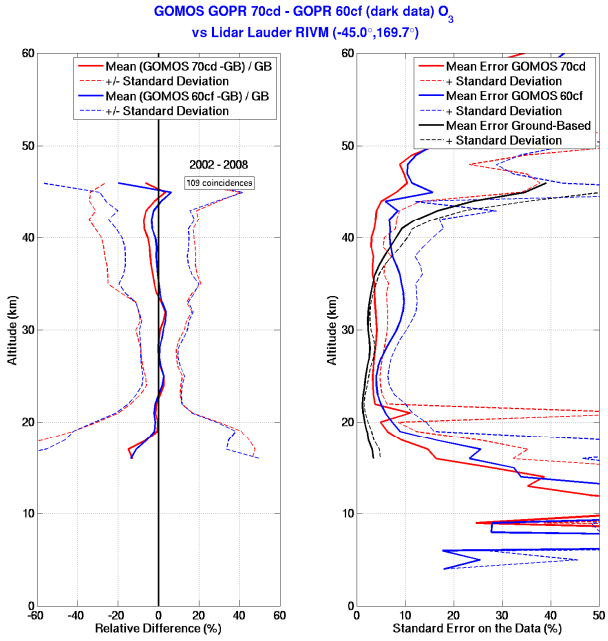

***Figure 22**: Same as Figure 16, but at the RIVM lidar station of Lauder, New Zealand.*

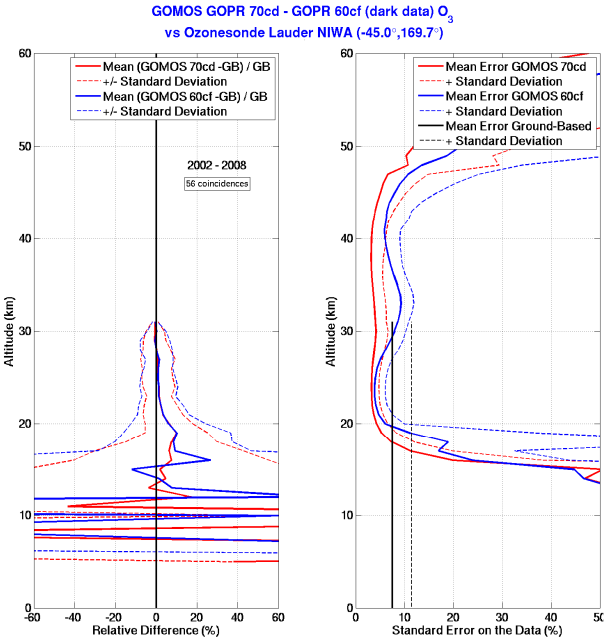

***Figure 23**: Same as Figure 16, but at the NIWA ozonesonde station in Lauder, New Zealand.*

Statistical analysis of meridian structures

Validation results obtained at 47 ozonesonde stations and at 11 lidar stations are summarised in Figures 24 and 25 respectively (*a*: GOPR 7.0cd; *b*: GOPR 6.0cf), where both dark and straylight GOMOS profiles have been used for comparisons. These figures report, on common altitude and latitude grids, the mean relative difference and corresponding standard deviation for the entire verification data set. Considering the zonal symmetry shown by the comparisons, results from the different stations have been averaged within bins of 5° of latitude. It should be noted that from the equator to about 40°S, only very few dark or straylight GOMOS profiles were found to coincide with ground-based ozonesonde and lidar observations. Figures 26 and 27 report, on the same template as figures 24 and 25, the median and the inter-percentile interval corresponding to 68 % of the data, for comparison.

In this analysis, the mean and median results are consistent with each other, and quasi-equivalent. The 68% inter-percentile is in general about 5% higher than the standard deviation, showing that the use of the standard deviation leads to an underestimation of the spread of the data.

In both analyses, the results obtained with the new GOPR prototype (7.0cd) are very similar to those obtained with the previous GOMOS data version 6.0cf:

- In the stratosphere, the mean relative difference and the median of the relative differences generally are smaller than 10 %. At Northern high latitudes, mean and median negative differences of about 5 to 10 % are observed. The standard deviation of the differences ranges within 10 % between 60°N and 60°S and increases up to 20 % at polar latitudes. The 68 % inter-percentile ranges within 15 % between about 40°N and 60°S and increases at higher latitudes, up to 25 % at polar latitudes.
- In the troposphere, the differences are very large (>50 %) at all latitudes, and their dispersion exceeds 50 %.

Conclusion

With respect to the previous version 6.0cf, the new GOPR prototype 7.0cd seems to improve slightly (a few percent maximum, not uniformly) the retrieval of GOMOS ozone profile data in the lower stratosphere (from 15-20 km to about 25 km). For all other data, the new prototype 7.0cd seems to offer, in the limits of this verification study, the same data quality as the one achieved with the reference version 6.0cf.

The error bars on the data have improved, mainly between 25 and 45 km altitude.

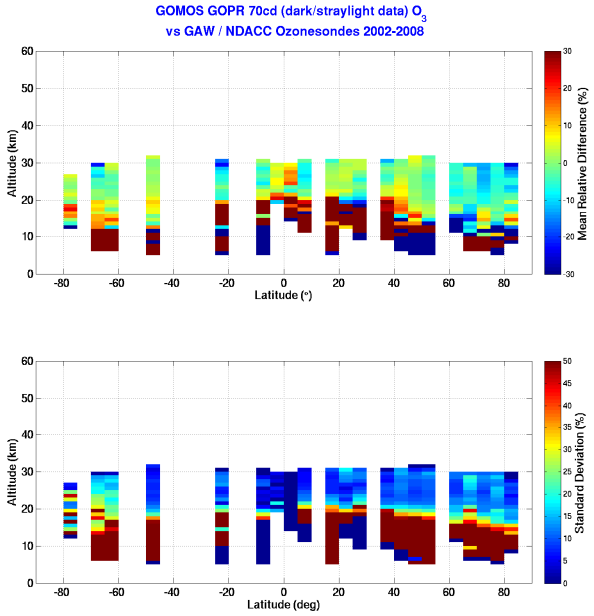

Figure 24a: *Altitude-latitude cross-section of the mean relative difference between GOMOS* ***(GOPR 7.0cd)*** *and ozonesonde observations at 47 GAW/NDACC/SHADOZ stations (top) and corresponding standard deviation (bottom).*

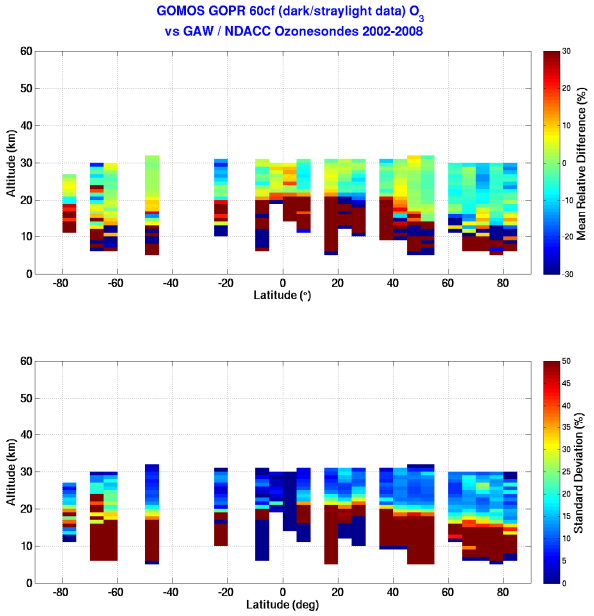

Figure 24b*: Same as Figure 24a, but for the reference GOMOS processor* ***(GOPR 6.0cf).***

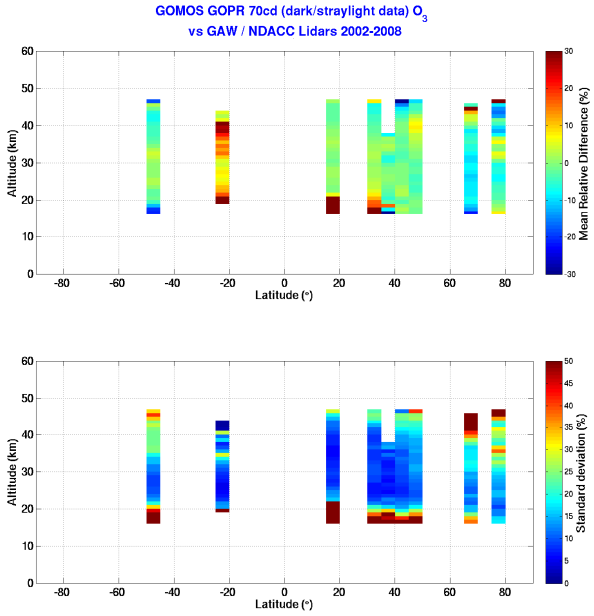

Figure 25a: *Same as Figure 24a, but for comparisons between GOMOS and lidar observations at 11 NDACC stations.*

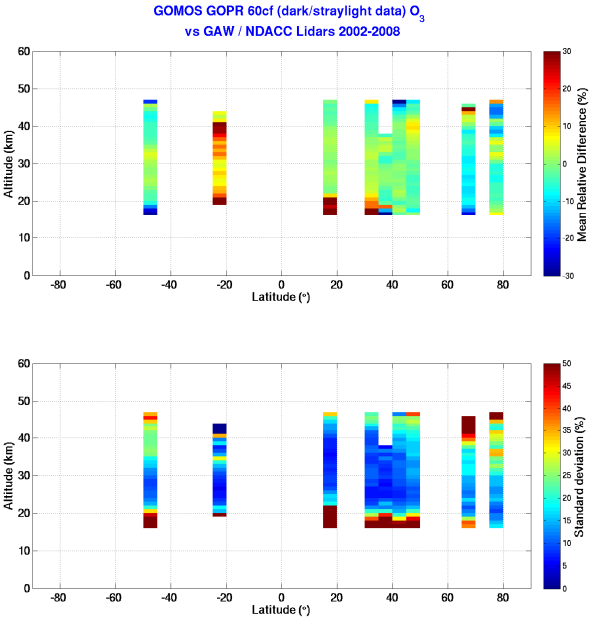

Figure 25b*: Same as Figure 25a, but for the reference GOMOS processor* ***(GOPR 6.0cf).***

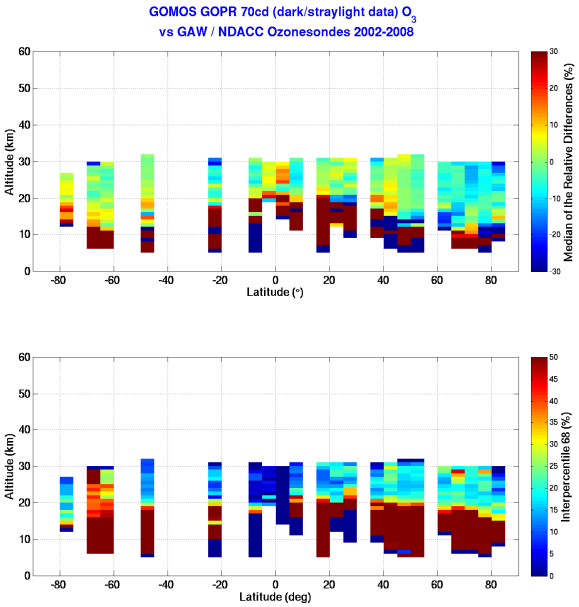

Figure 26a: *Altitude-latitude cross-section of the median of the relative difference between GOMOS* ***(GOPR 7.0cd)*** *and ozonesonde observations at 47 GAW/NDACC/SHADOZ stations (top) and corresponding inter-percentile interval corresponding to 68% of the data (bottom).*

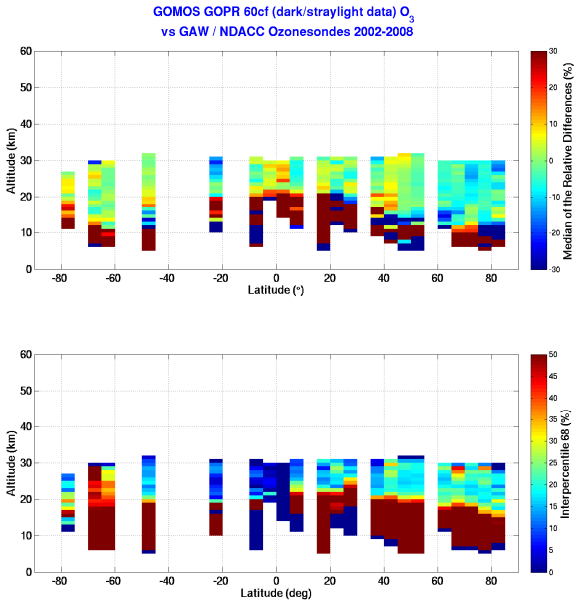

Figure 26b*: Same as Figure 26a, but for the reference GOMOS processor* ***(GOPR 6.0cf).***

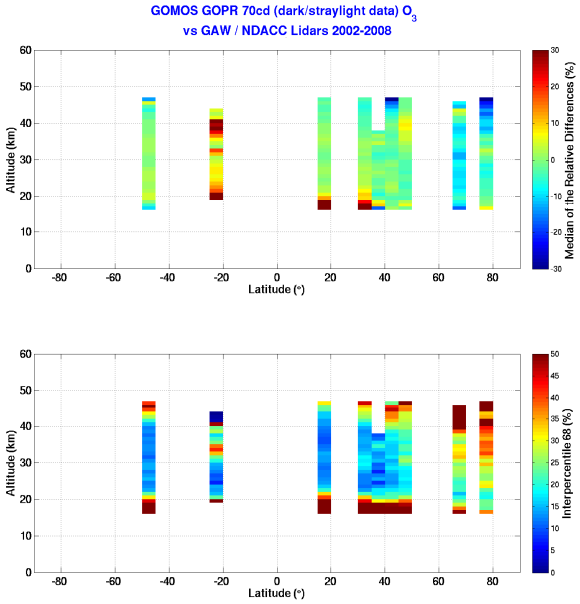

Figure 27a: *Same as Figure 26a, but for comparisons between GOMOS and lidar observations at 11 NDACC stations.*

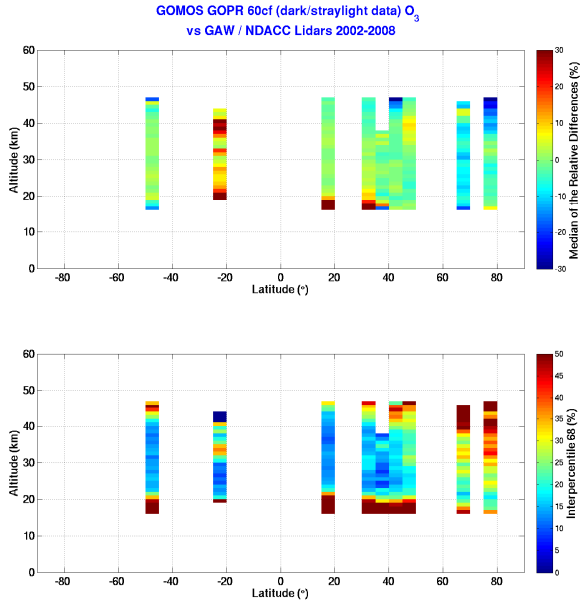

Figure 27b*: Same as Figure 27a, but for the reference GOMOS processor* ***(GOPR 6.0cf).***

Acknowledgements

This work has been funded by ESA's multi-mission validation project Multi-TASTE, and by the Belgian Federal Science Policy Office and ESA via the ProDEX project SECPEA. Ozonesonde and lidar data were obtained as part of the Network for the Detection of Atmospheric Composition Change (NDACC), Southern Southern Hemisphere ADditional OZonesondes (SHADOZ) and WMO's Global Atmosphere Watch (GAW), and are available via http://www.ndacc.org, http://croc.gsfc.nasa.gov/shadoz and http://www.woudc.org. We acknowledge the scientific and technical support of lidar and ozonesonde PIs and the staff at the stations, as well as the science and processing teams of the various satellite data.
In particular, we are grateful for the contributors from the following institutes, and thank their co-workers who contributed to generating these data:

- for ozonesonde data: M. Allaart (KNMI), S. B. Andersen (DMI), G. Bodeker (NIWA), H. Claude (DWD), H. De Backer (RMI), M. Gil and M. Yela (INTA), S. Godin-Beekmann,F. Goutail and M. Marchand (CNRS/LATMOS), R. Kivi and E. Kyrö (FMI), S. Oltmans (NOAA/ESRL), F. Posny (U. Reunion/LACy), R. Stubi (MCH);
- for lidar data: H. Claude and W. Steinbrecht (DWD), S. Godin-Beekmann (CNRS/LATMOS), G. H. Hansen (NILU), I. S. McDermid and T. Leblanc (NASA/JPL), H. Nakane (NIES), K. Strawbridge (MSC/EC), D. P. J. Swart (RIVM), and P. von der Gathen (AWI).

END OF DOCUMENT